The Synthesis of four Morphologies of TiO_2 through Temperature Control and Their Electrochemical Performance

Jie Qu, Jianning Ding[*] and Ningyi Yuan

School of Materials Science and Engineering, Jiangsu Collaborative Innovation Center of Photovolatic Science and Engineering and Jiangsu Province Cultivation base for State Key Laboratory of Photovoltaic Science and Technology, Changzhou University, Changzhou 213164, P. R. China
[*]E-mail: dingjn@cczu.edu.cn

TiO_2 nanoparticles (NP), muti-walled TiO_2 nanotubes, double-walled TiO_2 nanotubes (DWNT) and TiO_2 nanorods (NR) are prepared through hydrothermal method and followed calcination. The as prepared four samples were used as anode materials of Li-ion batteries. The electrochemical performance was carried out by galvanostatic method. It is found that DWNT presents the highest discharge and charge capacity and good rate capability; NP shows a relative high discharge and charge capacity but bad rate capability and NR shows the lowest discharge and charge capacity, but a good rate capability. The best electrochemical proformance of DWNT can be attributed to its unique two curled layers and resulting obvious pseudocapacitive storage feature.

1. INTRODUCTION

Due to its superior energy density, high rate capability and flexibility, lithium-ion batteries have been considered as the most promising power source in portable electronic devices [1-4]. However, there are still safety concerns with the graphite which is widely used as anodes in the commercial lithium-ion batteries. Many safety alternatives are prepared to replace graphite, such as TiO_2, SnO_2, NiO and etc. Titanium dioxide (TiO_2) due to its cost-effectiveness, nontoxicity, and obviously enhanced safety has showed tremendous potential [5-10]. Among all the polymorphs, TiO_2-B is the most attractive because of its unique three-dimensional crystal structure to offer more open voids and parallel channels, making it an excellent host material for Li-intercalation. Moreover, TiO_2-

B shows faster charge/discharge rates, higher charge capacity, and superior cyclability without significant distortion of the structure [11-13].

Besides polymorphs, other factors such as sizes, morphologies, crystallinity and et. al, also present significant effect on the electrode performance. For example, Zero-dimensional TiO_2 nanoparticles (NPs) can enable fast reaction kinetics of Li-ion storage because of the high specific surface are and abundant grain boundaries, while one-dimensional (1D) nanostructures show better electrochemical performance than NPs due to their specific geometric characteristics. So further research work to prepare different nanomaterials and to find out the electrochemical reaction mechanisms is necessary.

In this work, four morphologies of TiO_2-B nanomaterials (TiO_2 nanoparticles, muti-walled TiO_2 nanotubes, double-walled TiO_2 nanotubes, TiO_2 nanorods are prepared by a facile hydrothermal method by changing reaction temperatures. Electrochemical properties of the four nanomaterials were invested, and the different electrochemical features were also illustrated by the Cyclic voltammetry. Among the four samples, double-walled TiO_2 nanotube exhibit significantly enhanced electrode performance, including charge capacity, rate capability, and cyclability.

2. EXPERIMENTS

2.1. Synthesis of four morphologies of TiO₂ nanomaterials

TiO_2-B nanoparticles (NPs): NaOH (16 g) was dissolved in 40 ml of distilled water and then anatase TiO_2 powder (3 g) was added. The mixture was sonicated for 30 min, and then transferred to an airtight reactor and kept in an oven at 100 °C for 48 h. After cooling down to room temperature, the sample was treated with 0.1 M HCl for 24 h, and washed with distilled water several times. Then the product was kept in an oven at 60 °C for 48h, finally the product was transferred into tube furnace and heated at 300 °C for 2 h in Ar atmosphere.

Multi-walled TiO_2-B nanotubes, double-walled TiO_2-B nanotubes and TiO_2-B nanorods were synthesized the same as TiO_2-B nanoparticles, by adjusting the temperature to 130 °C, 150 °C and 180°C, respectively.

2.2. Structural analysis

The products were characterized by X-ray diffraction (XRD) (Rigaku D/max-2500 diffractometer) and transmission electron microscopy (TEM) (a FEI Tecnai 20 instrument).

2.3. Preparation of the electrodes

A mixture of 75 wt % of the active material, 18 wt % of acetylene black and 7 wt % of poly(tetrafluoroethylene, PTFE) were mixed to form a slurry and then pressed in to pellets. 1 M $LiPF_6$ dissolved in a volume ratio1:1 :1 mixture of ethylene carbonate (EC), ethyl methyl carbonate (EMC),

and dimethyl carbonate (DMC) was used as the electrolyte. The galvanostatic charge-discharge performance at different current densities was measured on a LAND-CT2001A instrument in the voltage range from 1.0 to 3.0 V. The cyclic voltammetry (CV) tests were employed on CHI600E electrochemical workstation.

3. RESULTS AND DISCUSSION

Fig. 1 shows the synthesis route of the four samples. Through hydrothermal method, using the same original materials, changing the reaction temperature to 100°C, 130°C, 150°C and 180°C, after annealing at 300°C for 2 h under argon, TiO_2-B nanoparticles, multi-walled TiO_2-B nanotubes, double-walled TiO_2-B nanotubes, TiO_2-B nanorods are prepared.
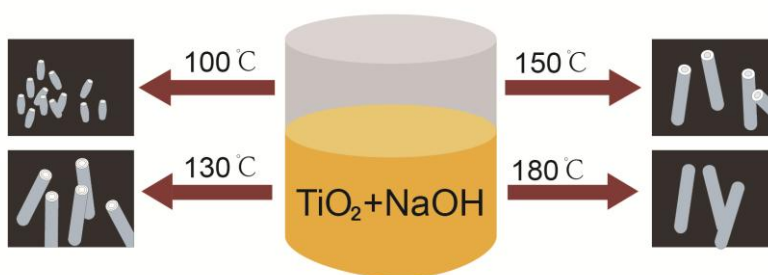

Figure 1. Schematic illustration of the synthesis route to four morphologies of TiO_2 nanomaterials.

As shown in Fig 2a, TiO_2 nanoparticles (NP) prepared at 100 °C are observed with a size of about 20 nm which are conglomerated into a group. When the reaction temperature rising to 130 °C TiO_2 nanotube morphology is observed. The length is about several hundred nanometers, the outer diameter is about 8-17 nm, while the inner diameter is about 7-10 nm. Such nanotubes are typically several layers (MWNT). TiO_2 nanotubes with two curled layers (DWNT) are occured when hydrothermal temperature changing to 150 °C with outer diameters of about 8-10 nm and inner diameters of about 5 nm. It should also be mentioned that the interlayer spacing for double-walled TiO_2-B nanotubes is a little larger than for multilayer TiO_2 nanotubes. Such unique structure of the as-prepared sample contributes to its excellent rate performance as demonstrated below. Solid TiO_2 nanorods (NR) are got when hydrothermal temperature changing to 180 °C. The length is about several micrometers, while the diameter is about 150 nm. From the image insert in Fig. 2d, the interference fringe spacing of the nanorods can be detected which is about 0.37 nm. This result is in consistent with the (101) plane of TiO_2-B which further confirms the formation of the TiO_2-B.
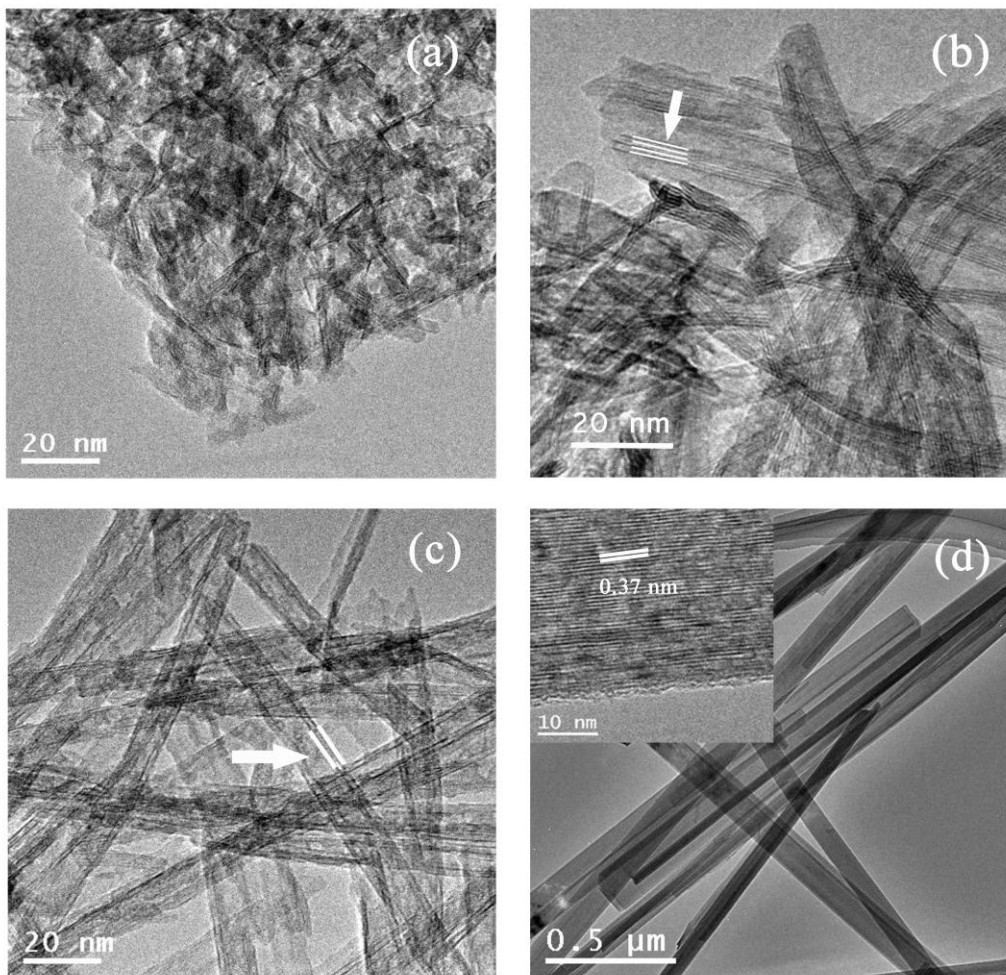
Figure 2. TEM images of four morphologies of TiO_2-B based materials, for which during the hydrothermal process the experimental conditions are 100 ^{o}C (a), 130 ^{o}C (b), 150 ^{o}C (c) and180 ^{o}C (d).
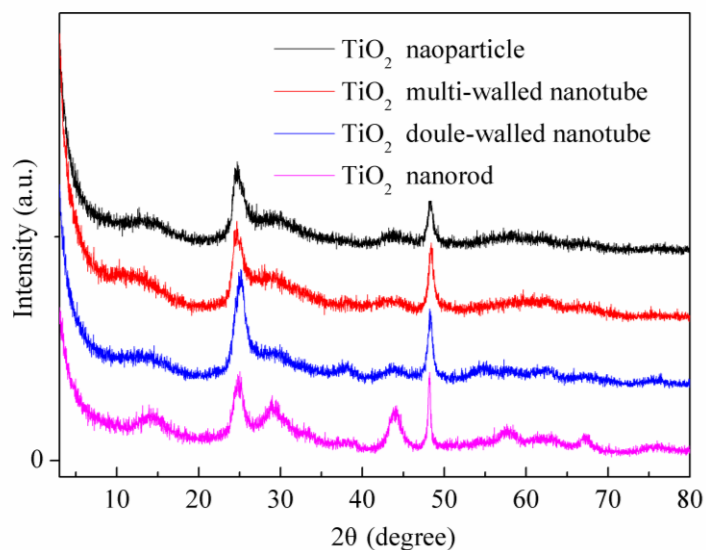

Figure 3. XRD data of four morphologies of TiO_2-B based materials.

XRD tests were employed to reveal the composition and structure of the four samples. Two

obvious diffraction peaks at about 25 and 48º are detected corresponding to (110) and (020) of TiO_2-B. But for NR, two additional peaks which appeared at 29 and 44 º are observed, which are also indexed as TiO_2-B. The peaks here of all samples are broadened which are typical features of nanomaterials. From the above results, it can be concluded that all the samples here are TiO_2-B phase [14-17].
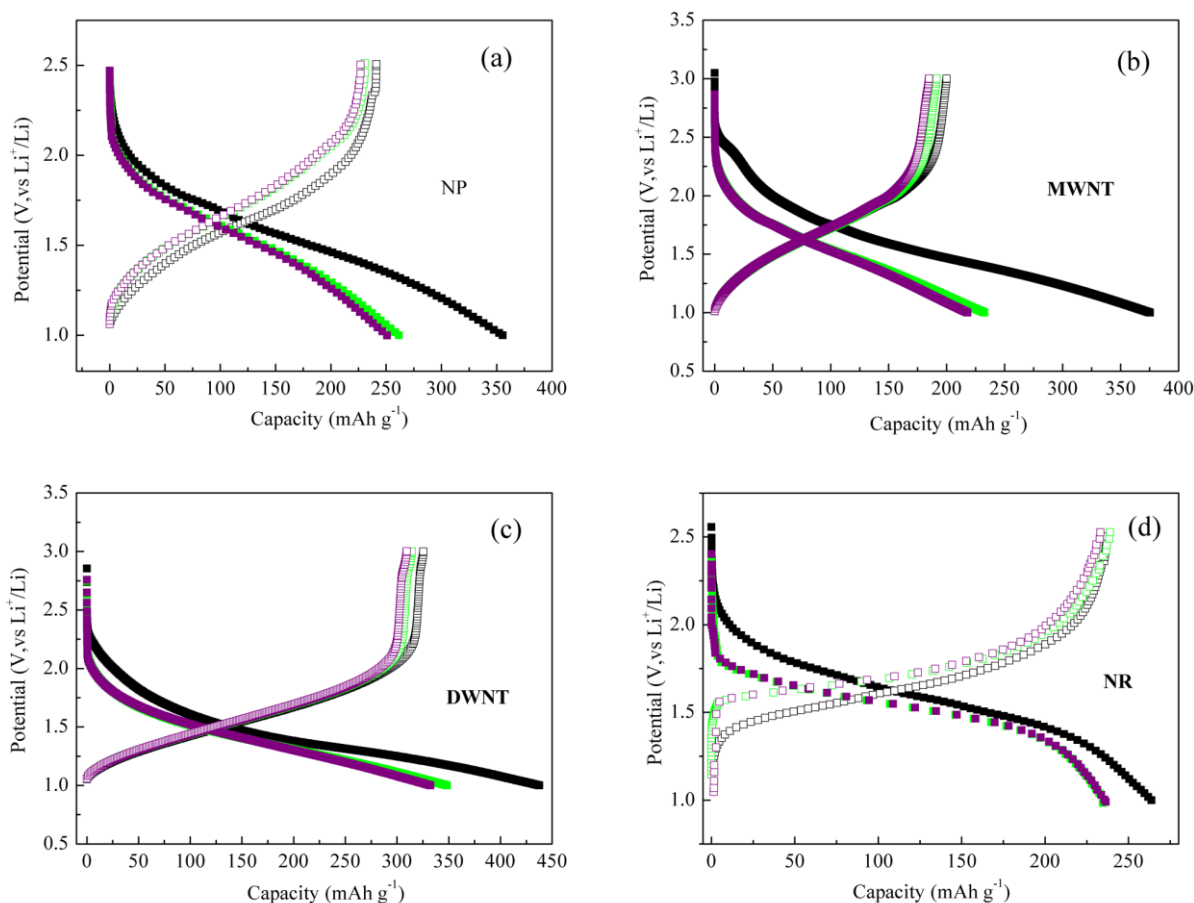

Figure 4. The potential-capacity plots for both discharge and charge processes during the first three cycles for four TiO_2-B electrodes.

Fig 4 shows the potential-capacity curves of the first three discharge-charge processes at the current density of 50 mAg^{-1}. Among the four samples, DWNT shows the highest first discharge and charge capacity, which is 437.5 and 325.5 mAhg^{-1}. While NR shows the lowest first discharge and charge capacity, which is 263.8 and 236.9 mAhg^{-1}. The irreversible capacity in the first cycle is 115.2 mAhg^{-1} for NP, 26.9 mAhg^{-1} for NR, 112.7 mAhg^{-1} for MWNT and 112 mAhg^{-1} for DWNT. NP, MWNT and DWNT show a relative large irreversible capacity in the first cycle caused by reactions between the surface of the samples and the electrolyte, which is a common phenomenon for nanostructured electrodes [18-21]. However for NR, the irreversible capacity is much lower than for other three samples.
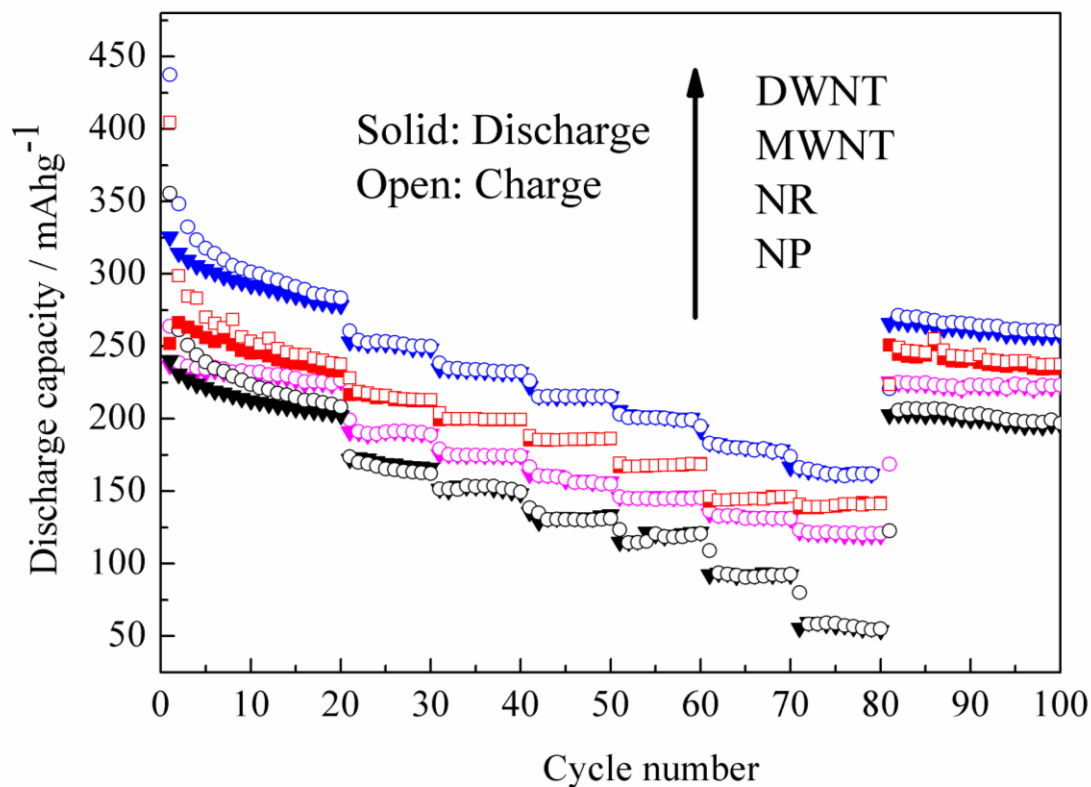
Figure 5. Cycle performance of four morphologies of TiO_2-B electrodes at various charge/discharge rates of 50 mAg^{-1} for the first 20 cycles, then at 250 mAg^{-1}, 500 mAg^{-1}, 750 mAg^{-1}, 1000 mAg^{-1}, 1500 mAg^{-1}, 2000 mAg^{-1} for 10 cycles each, and finally at 50 mAg^{-1} for 20 cycles

To text the cyclability and rate capability of the samples cycling test beyond various current rate are carried out in Fig 5. The capacities of the four materials decrease with increasing current densities. And after the first 20 cycles, the capacity degradation is less than 0.1% after each cycle. At the rate of 2000 mAg^{-1}, the capacity of DWNT can still keep at 163 mAhg^{-1}. After changing the rate back to 50 mAg^{-1}, the capacity is almost fully recovered to 261 mAhg^{-1}. However, for NP at the rate of 2000 mAg^{-1}, the capacity is only about 59 mAhg^{-1} much lower than other three sample (121 mAhg^{-1} for NR and 160 mAhg^{-1} for MWNT), but it can also fully recover to 202 mAhg^{-1} after changing to the rate of 50 mAg^{-1} (221 mAhg^{-1} for NR and 241 mAhg^{-1} for MWNT). Of the four samples, DWNT owns the highest discharge and charge capacity and good rate capability, while NP shows a relative high discharge and charge capacity but bad rate capability. Such excellent rate capability can attribute to the unique two curled layers of as-prepared TiO_2-B nanotubes. A double-walled structure with a larger spacing can facilitate the fast transport of lithium ions throughout the entire material, and further shorten the transport distance of electrons and ions, thus leading to a better electrochemical performance [10]. Eventhough NR shows the lowest discharge and charge capacity, it presents a good rate capability which due to its solid structure.
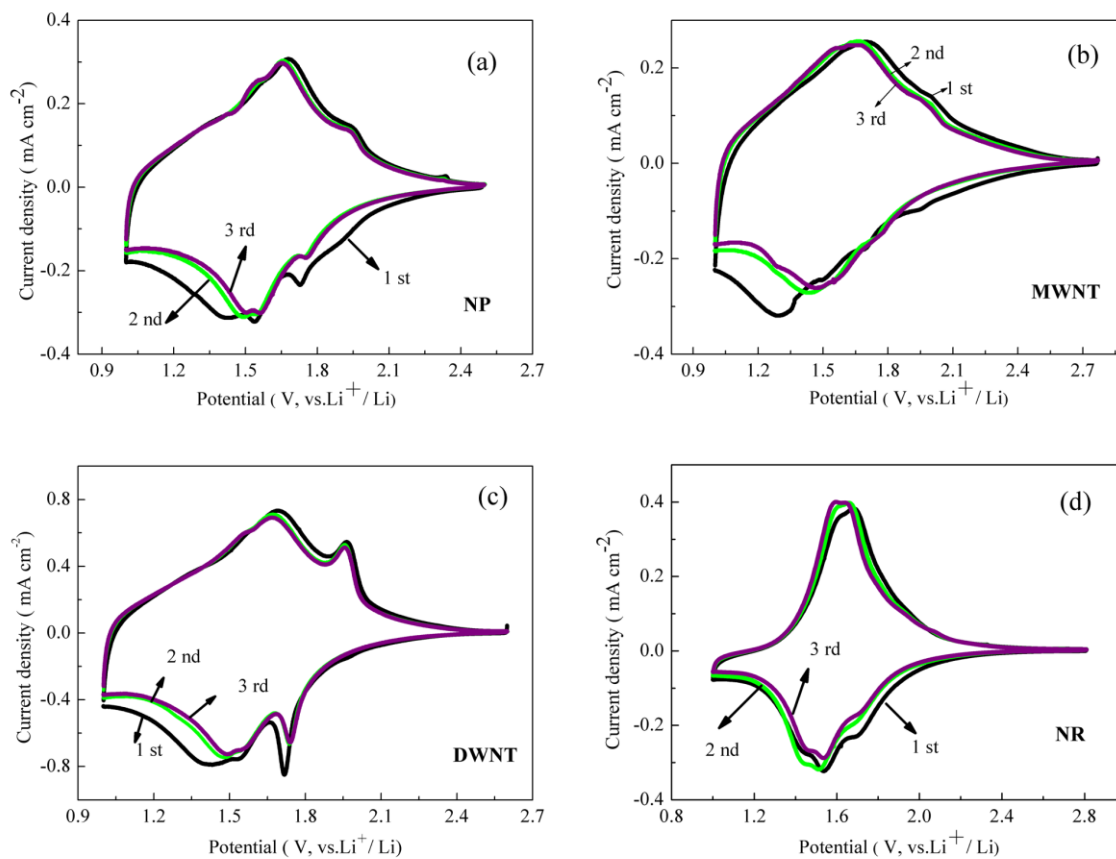
Figure 6. CV curves of the four TiO$_2$-B materials (scan rate of 0.1 mVs^{-1}).

Initial CV tests of the four samples at a slow scan rate of 0.1 mVs^{-1} are presented in Fig 6. All samples display a pair of redox peaks, at 1.54 V/[1.51, 1.68] V for NP, 1.28 V/[1.60, 1.68] V for MWNT, 1.41 V/[1.55, 1.69] V for DWNT, and 1.54 V/[1.6, 1.68] V for NR, corresponding to the lithium-ion intercalation/deintercalation in TiO$_2$-B. For all samples the anodic peak consists of two shoulder peaks, which also reported in previous papers and ascribed to the Li extraction processes associated with different sites [22-23]. Another pair of small peaks at 1.73/1.95 V for NP, 1.71/1.97 V for MWNT and 1.72/1.96 V for DWNT is assigned to the impurity of anatase TiO$_2$ [22, 24]. There is a significant current-intensity loss between the first and the second cycle for NP, MWNT and DWNT and fairly small current-intensity loss for NR; in addition, almost no lost are detected in the second and third cycle. This result is in consistent with the capacity data in Fig 5.

Furthermore, the CVs at different scan rates are given to reveal the reason of such difference in electrochemical performance in Fig 7. All four samples show slight peak potential shifts, indicating no serious electrode polarization or phase transition.
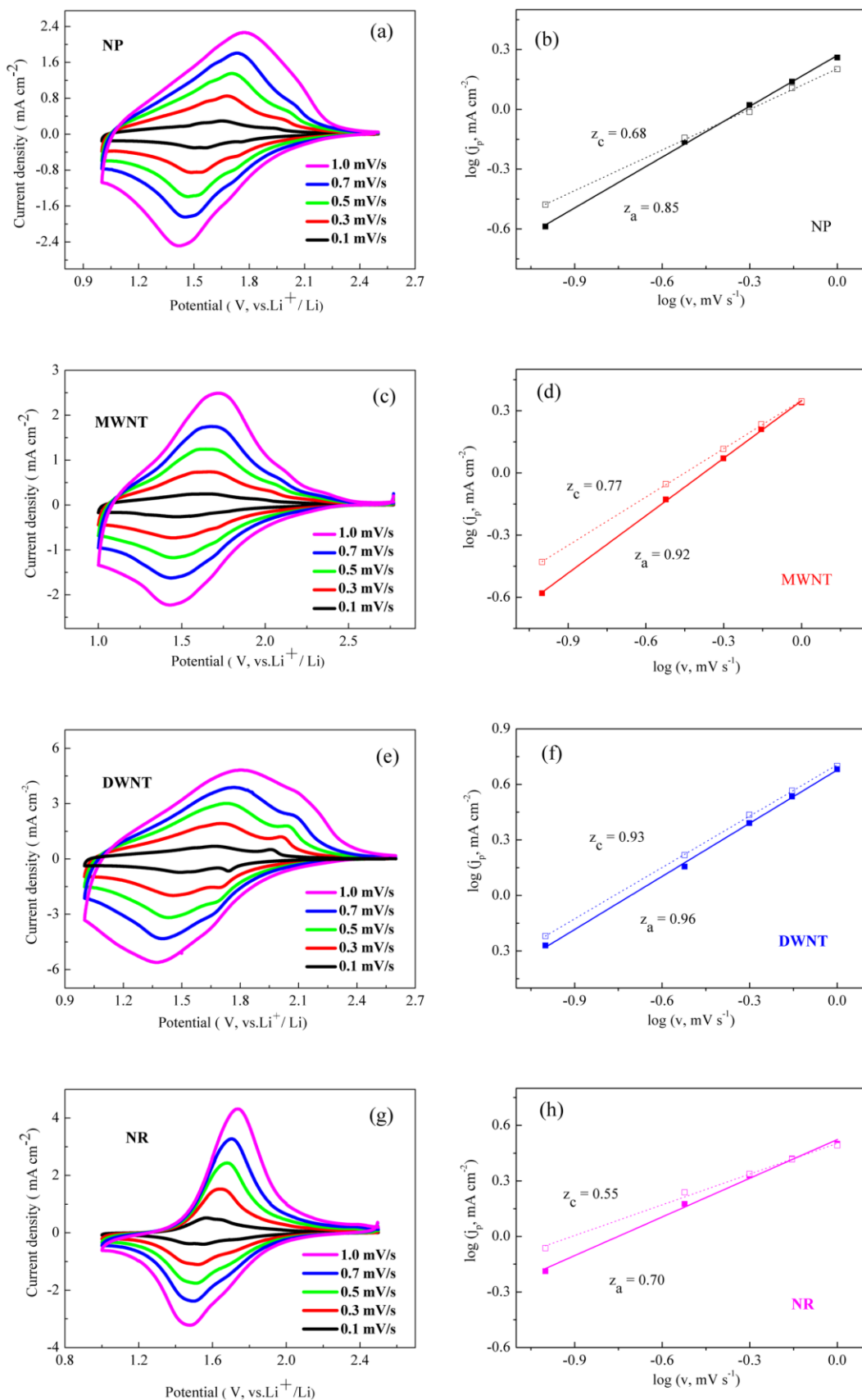
Figure 7. Cyclic voltammograms of four TiO$_2$-B materials at five different scan rates and the plots of log (j$_p$, mA/cm^2) ~ log (v, mV/s) based on the cyclic voltammograms.

The nature of anodic and cathodic currents can be characterized by investigating the peak current (j_p) with the scan rate (v) according to equation 1 [25]:

$$j_p \propto v^z \quad (1)$$

When the z value is ca. 0.5, it indicates the dominant process is a Li^+ insertion process; while a value between 0.8-1 implies a surface-controlled current [25]. z_a value for the anodic peak is about 0.96 for DWNT, 0.92 for MWNT, 0.85 for NP and 0.70 for NR. For DWNT and MWNT, z_a value is almost close to 1, indicating a predominant pseudo-capacitive process[26-27]. And the z_c value is about 0.93 for DWNT, 0.77 for MWNT, 0.68 for NP and 0.55 for NR. For DWNT, the value is also close to 1, implying the fast Li ion transport even during the lithiation process, which due to its unique two curled layers offering a larger spacing. And in contrast, the value of NR is almost close to 0.5, which means the lithiation process is mainly governed by the reaction on the surface. While the other two materials show z_c values around 0.7, which indicates that diffusion in the bulk and the reaction on the surface together govern the process [25].

4. CONCLUSIONS

In conclusion, four different morphologies of TiO_2 nanomaterials (NP, MWNT, DWNT and NR) are prepared through hydrothermal method by changing reaction temperatures. DWNT presents the highest discharge and charge capacity and good rate capability. While NP shows a relative high discharge and charge capacity but bad rate capability. And NR shows the lowest discharge and charge capacity, but a good rate capability. For DWNT such excellent rate capability can be attributed to the unique two curled layers which offer a larger spacing facilitating the fast transport of lithium ions and further shortening the transport distance of electrons and ions. For NR the good rate capability due to its solid structure. Further investigations indicate a nature of the pseudocapacitive current and a fast Li ion transport during the lithiation/delithiation process for DWNT.

References

1. J. M. Tarascon, M. Armand, *Nature*, 414 (2001) 359-367.
2. F. Y. Cheng, J. Liang, Z. L. Tao, J. Chen, *Adv. Mater*, 23 (2011) 1695-1715.
3. J. Máca, J. Libich, M. Sedlaříková, J. Vondrák, A. S. Fedorková, *Int. J. Electrochem. Sci,* 10 (2015) 5264-5275.
4. L. Liu , M. An, P. Yang, J. Zhang, *Int. J. Electrochem. Sci,* 10 (2015) 1582-1594.
5. G. Liu, J. Qu, H. Wang, *J. Alloys Compd,* 578 (2013) 345-348.
6. S. G. Lee, H. Deng, J. Hu, L. Zhou, H. Liu, *Int. J. Electrochem. Sci,* 8 (2013) 2204-2219.
7. H. B. Wu, J. S. Chen, H. H. Hng, X. W. Lou, *Nanoscale*, 4 (2012) 2526-2542.

8. M. Zhen, L. Su, Z. Yuan, L. Liu, Z. Zhou, *RSC Adv*, 3 (2013) 13696-13701.
9. B. Han, Y. Lee, S. Kim, B. Hwang, S. Kim, W. Kim, K. Park, *Int. J. Electrochem. Sci,* 8 (2013) 8264-8271.
10. J. Qu, Q. D. Wu, Y. R. Ren, Z. Su, C. Lai, J. N. Ding, *Chem. Asian J*, 7 (2012) 2516-2518.
11. R. Marchand, L. Brohan, M. Tournoux, *MRS Bull,* 15 (1980) 1129-1133.
12. M. Tournoux, R. Marchand, L. Brohan, *Prog. Solid State Chem,* 17 (1986) 33-52.
13. J. Qu, J. E. Cloud, Y. Yang, J. Ding, N. Yuan, *ACS Appl. Mater. Interfaces,* 6 (2014) 22199-22208.
14. G. Armstrong, A. R. Armstrong, J. Canales, P. G. Bruce, *Electrochem. Solid-state Lett*, 9 (2006) A139-A143.
15. J. M. Li, W. Wan, H. H. Zhou, J. J. Li, D. S. Xu, *Chem. Commun*, 47 (2011) 3439-3441.
16. Q. J. Li, J. W. Zhang, B. B. Liu, M. Li, R. Liu, X. L. Li, H. L. Ma, S. D. Yu, L. Wang, Y. G. Zou, Z. P. Li, B. Zou, T. Cui, G. T. Zou, *Inorg. Chem*, 47 (2008) 9870-9873.
17. A. R. Armstrong, G. Armstrong, J. Canales, P. G. Bruce, *Angew. Chem., Int. Ed,* 43 (2004) 2286-2288.
18. G. Armstrong, A. R. Armstrong, J. Canales, P. G. Bruce, *Chem. Commun*, (2005) 2454-2456.
19. A. G. Dylla, J. A. Lee, K. J. Stevenson, *Langmuir*, 28 (2012) 2897-2903.
20. H. G. Jung, C. S. Yoon, J. Prakash, Y. K. Sun, *J. Phys.Chem. C*, 113 (2009) 21258-21263.
21. S. Brutti, V. Gentili, H. Menard, B. Scrosati, P. G. Bruce, *Adv. Energy Mater*, 2 (2012) 322-327.
22. M. Zukalova, M. Kalbac, L. Kavan, I. Exnar, M. Gräetzel, *Chem. Mater,* 17 (2005) 1248-1255.
23. A. G. Dylla, P. H. Xiao, G. Henkelman, K. J. Stevenson, *J. Phys. Chem. Lett,* 3 (2012) 2015-2019.
24. C. J. Chen, X. L. Hu, Z. H. Wang, X. Q. Xiong, P. Hu, Y. Liu, Y. H. Huang, *Carbon,* 69 (2014) 302-310.
25. V. Augustyn, J. Come, M. A.Lowe, J. W. Kim, P. L. Taberna, S. H.Tolbert, H. D. Abruna, P. Simon, B. Dunn, *Nat. Mater*, 12 (2013) 518-522.
26. J. R. Li, Z. L. Tang, Z. T. Zhang, Chem. Phys. Lett, 418 (2006) 506-510.
27. G. Nuspl, K. Yoshizawa, T. Yamabe, J. Mater. Chem, 7 (1997) 2529-2536.